International Journal of
Radiation Oncology
biology • physics

www.redjournal.org

Clinical Investigation: Gastrointestinal Cancer

Acute Cardiac Impairment Associated With Concurrent Chemoradiotherapy for Esophageal Cancer: Magnetic Resonance Evaluation

Masamitsu Hatakenaka, M.D., Ph.D.,*,¶ Masato Yonezawa, M.D.,* Takeshi Nonoshita, M.D.,* Katsumasa Nakamura, M.D., Ph.D.,* Hidetake Yabuuchi, M.D., Ph.D.,† Yoshiyuki Shioyama, M.D., Ph.D.,* Michinobu Nagao, M.D., Ph.D.,‡ Yoshio Matsuo, M.D., Ph.D.,* Takeshi Kamitani, M.D.,* Taiki Higo, M.D.,§ Kei Nishikawa, R.T.,‖ Taro Setoguchi, M.D., and Hiroshi Honda, M.D., Ph.D.***

*Departments of *Clinical Radiology, †Health Sciences, ‡Molecular Imaging and Diagnostic Radiology, and §Cardiovascular Medicine, Graduate School of Medical Sciences, Kyushu University, Fukuoka, Japan; ¶Department of Diagnostic Radiology, School of Medicine, Sapporo Medical University, Sapporo, Japan; ‖Radiology Center, Kyushu University Hospital, Kyushu University, Fukuoka, Japan; and **Department of Radiology, National Hospital Organization, Kokura Medical Center, Fukuoka, Japan*

Received Sep 8, 2011, and in revised form Nov 16, 2011. Accepted for publication Nov 30, 2011

Summary

Left ventricle (LV) function of 31 esophageal cancer patients received concurrent chemoradiotherapy (CCRT) was evaluated using magnetic resonance imaging. Patients were classified into two groups regarding mean LV dose. In low LV-dose group, LV ejection fraction decreased significantly. In high LV-dose group, LV end-diastolic volume index, stroke volume index, ejection fraction, and wall motion in segments 8–10

Purpose: To evaluate acute cardiac effects of concurrent chemoradiotherapy (CCRT) for esophageal cancer.

Methods and Materials: This prospective study was approved by the institutional review board, and written informed consent was obtained from all participants. The left ventricular function (LVF) of 31 patients with esophageal cancer who received cisplatin and 5-fluorouracil–based CCRT was evaluated using cardiac cine magnetic resonance imaging. The patients were classified into two groups according to mean LV dose. The parameters related to LVF were compared between before and during (40 Gy) or between before and after CCRT using a Wilcoxon matched-pairs single rank test, and parameter ratios (during/before CCRT, after/before CCRT) were also compared between the groups with a t test. Data were expressed as mean ± SE.

Results: In the low LV-dose group (n = 10; mean LV dose <0.6 Gy), LV ejection fraction decreased significantly (before vs. during vs. after CCRT; 62.7% ± 2.98% vs. 59.8% ± 2.56% vs. 60.6% ± 3.89%; $p < 0.05$). In the high LV-dose group (n = 21; mean LV dose of 3.6–41.2 Gy), LV end-diastolic volume index (before vs. after CCRT; 69.1 ± 2.93 vs. 57.0 ± 3.23 mL/m^2), LV stroke volume index (38.6 ± 1.56 vs. 29.9 ± 1.60 mL/m^2), and LV ejection fraction (56.9% ± 1.79% vs. 52.8% ± 1.15%) decreased significantly ($p < 0.05$) after CCRT. Heart rate increased significantly (before vs. during vs. after CCRT; 66.8 ± 3.05 vs. 72.4 ± 4.04 vs. 85.4 ± 3.75 beats per minute, $p < 0.01$). Left ventricle wall motion decreased significantly ($p < 0.05$) in segments 8 (before vs. during vs. after CCRT; 6.64 ± 0.54 vs. 4.78 ± 0.43

Reprint requests to: Masamitsu Hatakenaka, M.D., Ph.D., Sapporo Medical University, School of Medicine, Department of Diagnostic Radiology, Minami 1, Nishi 16, Chuo-ku, Sapporo City, Japan. Tel: (+81) 11-611-2111, ext. 3501; Fax: (+81) 11-633-6885; E-mail: mhatakenaka@sapmed.ac.jp

Conflict of interest: none.

Int J Radiation Oncol Biol Phys, Vol. 83, No. 1, pp. e67–e73, 2012
0360-3016/$ - see front matter
doi:10.1016/j.ijrobp.2011.12.018

decreased significantly. Heart rate increased significantly. CCRT for esophageal cancer impairs LV function from an early treatment stage.

vs. 4.79 ± 0.50 mm), 9 (6.88 ± 0.45 vs. 5.04 ± 0.38 vs. 5.27 ± 0.47 mm), and 10 (9.22 ± 0.48 vs. 8.08 ± 0.34 vs. 8.19 ± 0.56 mm). The parameter ratios of LV end-diastolic volume index, stroke volume index, wall motion in segment 9, and heart rate showed significant difference ($p < 0.05$) after CCRT between the groups.

Conclusions: Concurrent chemoradiotherapy for esophageal cancer impairs LVF from an early treatment stage. This impairment is prominent in patients with high LV dose.

Keywords: Esophageal cancer, Chemoradiotherapy, Cardiac function, Magnetic resonance imaging

Introduction

Concerns about radiation-related cardiac toxicities have been increasing, especially in patients with breast cancer who receive adjuvant radiotherapy (1, 2). Because such patients are expected to have a relatively good prognosis, cardiac toxicities that may cause death are clinically important. It would be meaningless that the patients lose their lives because of cardiac complications although primary breast cancers are completely cured.

Cisplatin and 5-fluorouracil–based concurrent chemoradiotherapy (CCRT) has become a standard treatment option for patients with unresectable or medically inoperable esophageal cancer. Although the survival rate for this treatment has not been satisfactory, it has been improving recently. Compared with breast cancer treatment, the radiation dose to the left ventricle (LV) in patients who receive CCRT for esophageal cancer is greater, and the extent of the LV receiving radiation is also larger. In this context, the importance of cardiac toxicities, including pericarditis, cardiovascular damage including cardiac infarction, and cardiomyopathy, has been increasing (3–6).

Ultrasonography and cardiac scintigraphy have been considered suitable methods for evaluating cardiac function noninvasively; however, magnetic resonance (MR) imaging including cine MR imaging has been accepted as the most reliable method (7). To our knowledge, however, the cardiac effects of CCRT for esophageal cancer have not yet been evaluated using cine MR imaging.

The purpose of this study was to evaluate the acute cardiac effects of CCRT for esophageal cancer by using cine MR imaging. Our hypothesis was that CCRT for esophageal cancer impairs left ventricular function (LVF) from an early treatment stage, and the impairment of LVF may be prominent in patients with mid- or lower thoracic esophageal cancer, in whom the LV dose is usually higher than in those with cervical or upper thoracic esophageal cancer.

Methods and Materials

Patients and treatment

This prospective study was approved by the institutional review board, and written informed consent was obtained from all patients. The 35 patients who were scheduled to receive CCRT for esophageal cancer in our department between November 2007 and June 2010 were consecutively enrolled in this study. Those who had a history of cardiovascular or neurovascular disease (1 case each of angina pectoris, aortic aneurysm, and cerebral infarct) and 1 patient who received radiotherapy alone because of renal dysfunction were excluded. Thus a total of 31 patients (25 male and 6 female; 47–85 years of age; median age 66 years) were included in this study. The locations of the disease were as follows: 8 cervical, 3 upper thoracic, 15 mid-thoracic, and 5 lower thoracic. The stages of the disease according to International Union Against Cancer 1997 criteria were as follows: 4 Stage I, 7 Stage II, 18 Stage III, and 2 Stage IV. The histologic diagnoses were all squamous cell carcinomas, except for 1 case of lymphoepithelial carcinoma. Patient characteristics are summarized in Table 1.

Radiotherapy was performed at a daily dose of 1.8–2.0 Gy, five times per week using a Varian 21EX linear accelerator (Varian Medical Systems, Palo Alto, CA). Radiotherapy was delivered through anteroposterior portals using 4-, 6-, or 10-MV photon beams with a T-shaped or I-shaped field including primary lesions and regional nodes to 40–41.4 Gy, and the boost was delivered through parallel opposed oblique portals avoiding the spinal cord. Twenty-five patients were treated by CCRT with a low-dose protocol (cisplatin 5 mg/m^2 bolus infusion and 5-fluorouracil 300 mg/m^2 24-h continuous infusion during radiotherapy), and the remaining 6 patients were treated with a standard-dose protocol (cisplatin 70 mg/m^2 bolus infusion on Day 1, and 5-fluorouracil 700 mg/m^2 24-h continuous infusion on Days 1–4; two cycles are given during radiotherapy). This study included two types of treatments: Type A included patients who received radical CCRT with a total radiation dose of 55.4–71 Gy ($n = 24$, 18 patients treated with a low-dose chemotherapy protocol and 6 patients with a standard-dose one). (Total radiation dose of approximately 60 Gy with 30 fractions is a standard CCRT for advanced esophageal cancer in Japan.) Type B included patients who received a total radiation dose of 40–41.4 Gy and were treated by surgery after CCRT ($n = 7$, all patients treated with a low-dose chemotherapy protocol). The treatment schema is shown in Fig. 1.

Patient classification according to LV dose

The patients were divided into two groups according to their mean total LV dose: a low LV-dose and a high LV-dose group. The contour of LV was defined and the mean LV dose was calculated with an Eclipse planning system (Varian Medical Systems). This procedure was performed by a radiation oncologist (T.N.) with 12 years' experience, who was blinded to the data of MR imaging. Representative dose distributions are shown in Fig. 2.

MR imaging

Magnetic resonance examination was performed with a 1.5-T system (Gyroscan Intera Achieva; Philips Medical Systems, Best,

Table 1 Patient characteristics according to LV dose

Parameter	Mean LV dose		*p*
	Low	High	
Age (y), mean ± SE	66.7 ± 9.1	63.8 ± 11.9	NS
Gender			
Male	7	18	NS
Female	3	3	
Stage			
I	0	4	NS
II	4	3	
III	6	12	
IV	0	2	
Location			
Cervical	7	1	<0.01
Upper thoracic	3	0	
Mid-thoracic	0	15	
Lower thoracic	0	5	
Cardiac risk factor			
Smoking (+)	5	15	NS
Smoking (−)	5	6	
Hypertension (+)	3	4	NS
Hypertension (−)	7	17	
Hypercholesterolemia (+)	0	1	NS
Hypercholesterolemia (−)	10	20	
BMI (kg/m^2), mean ± SE	21.1 ± 2.8	19.5 ± 2.4	NS
Chemotherapy			
Low dose	8	17	NS
Standard dose	2	4	

Abbreviations: LV = left ventricle; NS = nonsignificant ($p > 0.05$); BMI = body mass index.

The Netherlands), and a cardiac coil with five channels was used. The LVF was evaluated using cine MR imaging with 20 heart phases, a 350-mm field of view, 10-mm slice thickness, 0-mm slice gap, 192 × 184 matrix, 3.2-ms repetition time, 1.6-ms echo time, 55° flip angle, and balanced turbo field-echo sequence. The cine MR imaging was obtained before CCRT for all 31 patients, at a primary lesion dose of approximately 40 Gy for 27 patients, and after CCRT for 19 patients. The duration between the MR examination before CCRT and the start of CCRT was 0–11 days, and the median was 1 day. The duration between the MR examination after CCRT and the completion of CCRT was 0–12 days, and the median was 3 days. The exact radiation doses to the primary lesion at the MR examination performed at approximately

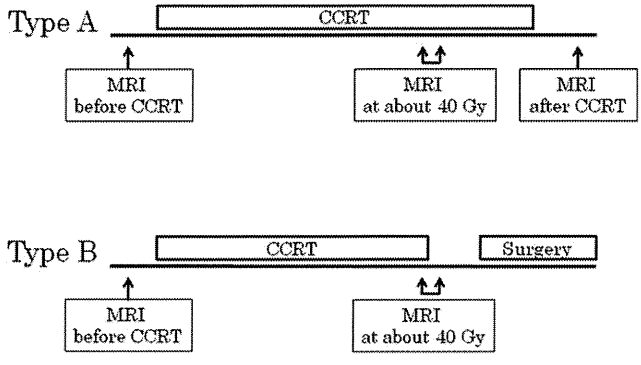

Fig. 1. Scheme of the treatments. CCRT = concurrent chemoradiotherapy; MRI = magnetic resonance imaging.

40 Gy and after CCRT were distributed from 34.2 to 43.4 Gy (median, 41.4 Gy) and from 60.0 to 71.4 Gy (median, 65.4 Gy), respectively. (Some patients received MR examination either at approximately 40 Gy or after CCRT.)

Data acquisition and analysis

Patient characteristics were compared as follows: age and body mass index were compared between low and high LV-dose groups using a *t* test, and other categoric data were compared using a χ^2 test. Probability (*p*) values of <0.05 were considered statistically significant.

The LVF analysis was performed with View Forum (Philips Medical Systems) and by M.Y. and K.N. in consensus (M.Y. has 8 years of experience in cardiac imaging, and K.N. has 15 years of experience in MR imaging). Both were blinded to the CCRT method used for each patient. Several parameters related to LVF (end-diastolic volume index [LV-EDVI], end-systolic volume index [LV-ESVI], stroke volume index [LV-STVI], ejection fraction [LV-EF], cardiac output index [COI], heart rate [HR], and LV wall motion [LV-WM] and LV wall thickening [LV-WT] at the mid-LV portion [segments 7–12 according to the American Heart Association]) were measured and compared between before CCRT and at approximately 40 Gy or after CCRT using a Wilcoxon matched-pairs single rank test. The parameter ratios of LV-EF, LV-EDVI, LV-ESVI, LV-STVI, HR, COI, LV-WM, LV-WT, and body weight at approximately 40 Gy (*i.e.*, the LV-EF, LV-EDVI, LV-ESVI, LV-STVI, HR, COI, LV-WM, LV-WT, and body weight at approximately 40 Gy divided by those before CCRT) and those after CCRT (LV-EF, LV-EDVI, LV-ESVI, LV-STVI, HR, COI, LV-WM, LV-WT, and body weight after CCRT divided by those before CCRT) were compared between the low and high LV-dose groups using a *t* test. A *p* value <0.05 was considered statistically significant. Data were expressed as the mean ± SE unless otherwise specified. To minimize the effects of height and body weight, LV-EDVI, LV-ESVI, LV-STVI, and COI (divided by body surface area) were used.

Results

Patient classification according to LV dose

The low LV-dose group included 10 patients and consisted of cervical and upper thoracic cancers. The mean LV dose was <0.6 Gy (mean, 0.37 Gy) at MR examination at approximately 40 Gy and <0.5 Gy (mean, 0.33 Gy) at MR examination after CCRT. The constitution of the patients undergoing cine MR imaging differed between the MR examinations at approximately 40 Gy and that after CCRT; therefore, the mean LV dose at MR examination at approximately 40 Gy was greater than that at MR examination after CCRT. The high LV-dose group included 21 patients and consisted of mid- and lower thoracic cancers, including 1 case of cervical cancer with extended lymph node metastasis. The mean LV dose was distributed from 3.6 to 29.4 Gy (mean, 15.5 Gy; median, 15.6 Gy) at MR examination at approximately 40 Gy and from 4.6 to 41.2 Gy (mean, 18.1 Gy; median, 16.3 Gy) at MR examination after CCRT. There were no significant differences with respect to age, gender, disease stage, cardiac risk factors, or chemotherapy method between patients receiving low and high LV doses, but the primary lesion location did differ significantly between the two dose groups. The

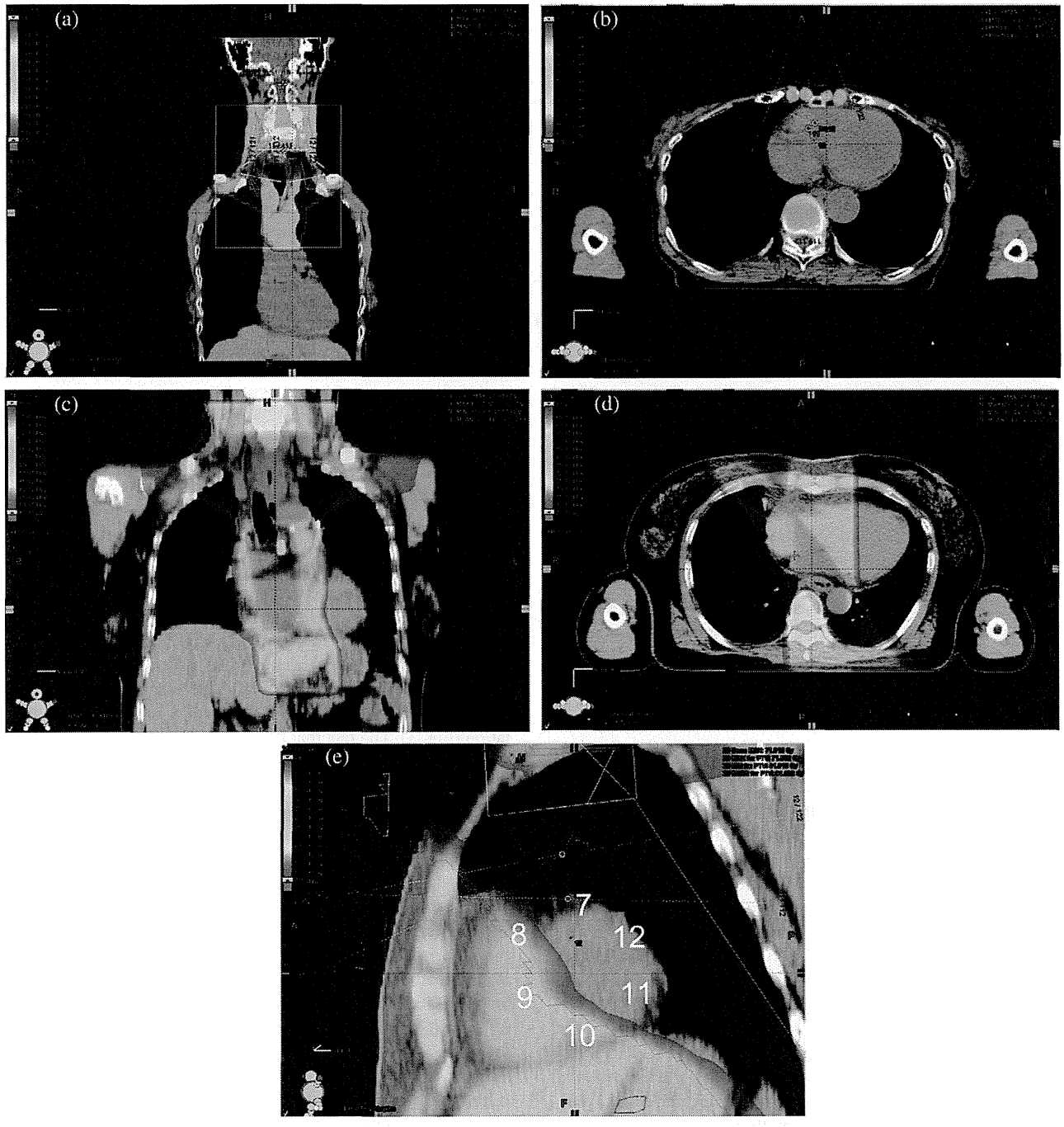

Fig. 2. Representative dose distributions of cases in the low left ventricle (LV)-dose (a, b) and high LV-dose (c, d, e) group. Coronal (a) and axial (b) views of dose distribution in a case with cervical esophageal cancer. Left ventricle receives no direct radiation. Coronal (c), axial (d), and short LV axis (e) views of dose distribution in a case with mid-thoracic esophageal cancer. A summation of the anteroposterior and parallel opposed oblique fields is shown. Numbers indicate the cardiac segments according to the American Heart Association classification (e).

classification of patient characteristics according to LV dose is summarized in Table 1.

Comparison of parameters related to LVF between before CCRT and at approximately 40 Gy or after CCRT

In the low LV-dose group, the LV-EF decreased significantly ($p < 0.05$) both at approximately 40 Gy (59.8% ± 2.56%) and after CCRT (60.6% ± 3.89%) compared with before CCRT (62.7% ± 2.98%). No other parameters showed significant change. In the high LV-dose group, the LV-EF, LV-EDVI, and LV-STVI decreased significantly ($p < 0.05$) after CCRT compared with before CCRT. The HR increased significantly ($p < 0.01$) both at approximately 40 Gy and after CCRT compared with before CCRT. The LV-WM of segments 8, 9, and 10 decreased significantly ($p < 0.05$) both at approximately 40 Gy and after CCRT compared with before CCRT. No other parameters showed significant change. The data are summarized in Table 2.

Table 2 Change of left ventricular function in the high LV-dose group

Parameter	MR examination		
	Before CCRT	40 Gy	After CCRT
LV-EF (%)	56.9 ± 1.79	55.0 ± 1.42	52.8 ± 1.15*
LV-EDVI (mL/m^2)	69.1 ± 2.93	64.7 ± 2.49	57.0 ± 3.23†
LV-STVI (mL/m^2)	38.6 ± 1.56	35.2 ± 1.11	29.9 ± 1.60†
HR (beats/min)	66.8 ± 3.05	72.4 ± 4.04†	85.4 ± 3.75†
LV-WM (mm) in segment 8	6.64 ± 0.54	4.78 ± 0.43†	4.79 ± 0.50*
LV-WM (mm) in segment 9	6.88 ± 0.45	5.04 ± 0.38†	5.27 ± 0.47†
LV-WM (mm) in segment 10	9.22 ± 0.48	8.08 ± 0.34*	8.19 ± 0.56*

Abbreviations: LV = left ventricle; MR = magnetic resonance; CCRT = concurrent chemoradiotherapy; EF = ejection fraction; EDVI = end-diastolic volume index; STVI = stroke volume index; HR = heart rate; WM = wall motion.

* $p < 0.05$ vs. before CCRT.

† $p < 0.01$ vs. before CCRT.

Comparison of parameter ratios related to LVF between the low and high LV-dose groups

Significant differences ($p < 0.05$) in the parameter ratios between the low and high LV-dose groups were observed only in the values calculated after CCRT for LV-EDVI ratio, LV-STVI ratio, HR ratio, and LV-WM ratio of segment 9. No other parameters, including LV-EF ratio and body weight ratio, showed significance either at approximately 40 Gy or after CCRT. The results are summarized in Fig. 3.

Discussion

The results of this study indicate that LVF, both systolic and diastolic, is impaired from an early treatment stage in patients who received cisplatin and 5-fluorouracil–based CCRT for esophageal cancer. The cardiac toxicity of CCRT for esophageal cancer has been considered as one of the late toxicities (3, 8, 9); however, the results of this study reveal that parameters related to LVF decrease significantly immediately after CCRT compared with those before CCRT. To our knowledge, this is the first report to detect acute cardiac dysfunction, that is a reduction in LV-EF, LV-EDVI, LV-STVI, and LV-WM and an increase in HR, using cine MR imaging in patients who received CCRT for esophageal cancer. As for LV-EF, a significant reduction has also been reported in patients who received platinum-based chemoradiotherapy for esophageal cancer after treatment, according to multigated acquisition scanning (10, 11).

Cisplatin and 5-fluorouracil–based chemotherapy impairs systolic LVF. Systolic dysfunction detected as a reduction in LV-EF was observed both in the low LV-dose and high LV-dose groups in the present study. This suggests that the decrease in LV-EF may happen irrespective of the LV radiation dose. The fact that the ratios of LV-EF after CCRT (*i.e.*, the LV-EF after CCRT divided by the LV-EF before CCRT) showed no significant difference between the low and high LV-dose groups supports this interpretation (Fig. 3). The fact that 5-fluorouracil has been reported to induce ischemic syndrome, arrhythmia, and cardiomyopathy (12, 13) is not discrepant with our results. Late cardiovascular complications by cisplatin have also been reported (14). Platinum-based therapies are also known to increase the risk of thrombus formation (15–17).

Direct radiation to LV might impair diastolic LVF dominantly. In the high LV-dose group, the LV-EDVI and LV-STVI decreased significantly after CCRT (Table 2), and the LV-ESVI showed no significant change. Further, the impairment of LV-WM was detected both at approximately 40 Gy and after CCRT only at segments 8, 9, and 10 (Table 2), where the radiation dose is higher than at the other segments (Fig. 2). These results suggest that direct radiation to LV might predominantly impair diastolic function through a restriction of wall motion in the radiated areas. The result that a significant difference was observed in the ratio of LV-EDVI, LV-STVI, and LV-WM in segment 9 after CCRT between the low and high LV-dose groups supports this interpretation (Fig. 3). The fact that the ratio of LV-EF after CCRT showed no significant difference between the low and high LV-dose groups also supports this interpretation (Fig. 3). Radiation-induced direct myocardial damage, that is, a significant elevation in troponin I and brain natriuretic peptide during radiotherapy for lung and breast cancer, has been reported (18). In the present study, T2-weighted images with fat saturation were obtained in some cases as to detect edematous or fibrotic change of LV; however, no signal increase or decrease in the irradiated areas compared with the nonirradiated areas was observed visually (data not shown). We suspected that a difference in the degree of dehydration related to CCRT between the low and high LV-dose groups may have affected the results, with respect to the decrease in LV-EDVI and increase in HR, and we therefore compared the ratio of body weight between these two groups. However, no significant difference was observed. We consider that a difference in the degree of dehydration related to CCRT does not affect the results. Late diastolic dysfunction and its association with stress-induced ischemia and a worse prognosis have been reported in patients who received mediastinal radiation of >35 Gy for Hodgkin's disease (19). On the other hand, in breast cancer, systolic LV dysfunction, a regional strain and strain rate reductions, immediately after adjuvant radiotherapy has been reported in a study assessing LVF using cardiac ultrasonography (20). The difference in the extent and location of LV that receive radiation may contribute to the difference in results between breast and esophageal cancer. The LV area included in the radiation field is usually restricted to the apex in only left-sided breast cancer. We also consider that the lack of change in COI in the high LV-dose group either at approximately 40 Gy or after CCRT was probably due to a compensation for the decrease in LV-STVI by the elevation of HR. The fact that LV-STVI and HR showed the opposite

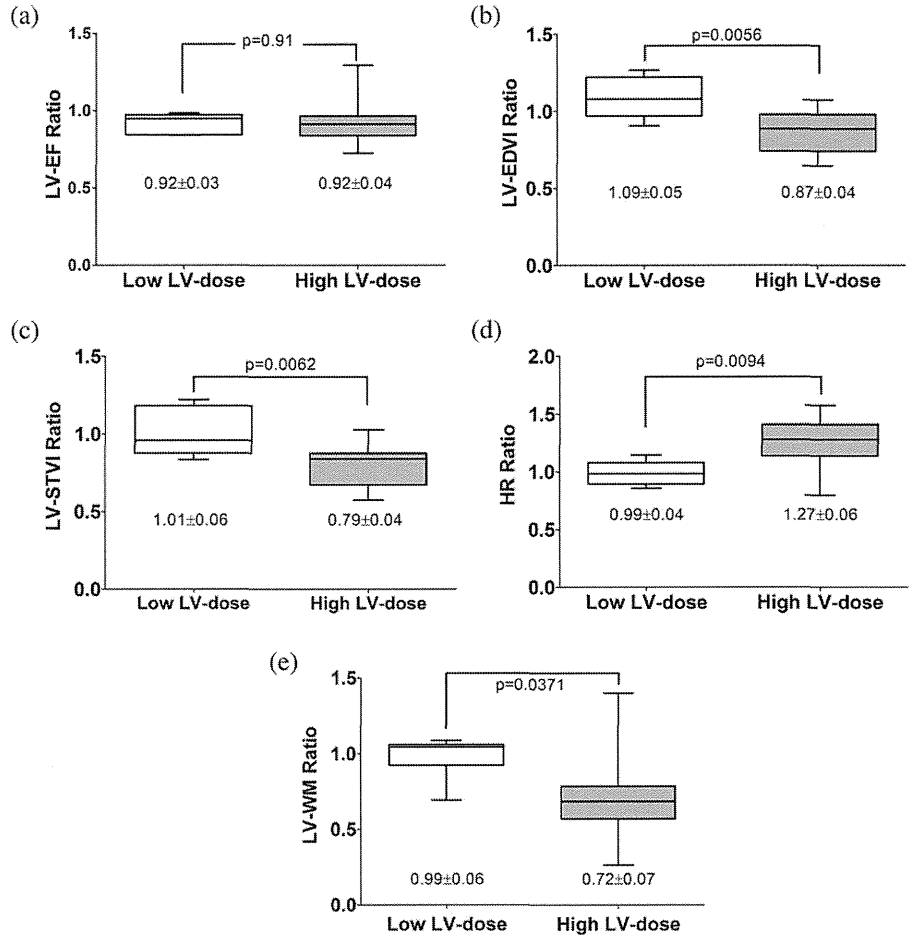

Fig. 3. Comparison of parameter ratios (after concurrent chemoradiotherapy [CCRT]/before CCRT) between low left ventricle (LV)-dose and high LV-dose groups. Left ventricle ejection fraction (LV-EF) ratio (a), LV end-diastolic volume index (LV-EDVI) ratio (b), LV stroke volume index (LV-STVI) ratio (c), heart rate (HR) ratio (d), and LV wall motion (LV-WM) ratio of segment 9 (e) are shown.

directional changes after CCRT supports this interpretation (Table 2 and Fig. 3).

The results of this study are limited in that the total number of patients is small. A more comprehensive study with a larger number of patients and detailed evaluation on cardiac function, including diastolic LVF, will be needed to reach a definitive conclusion. Further, a study with longer observation time may also be needed to determine whether the acute cardiac impairment observed in this study continues to correlate with late cardiac toxicities.

In conclusion, cisplatin and 5-fluorouracil–based CCRT for esophageal cancer impairs LVF from an early treatment stage, and this impairment is prominent in the high LV-dose group.

References

1. Evans ES, Prosnitz RG, Yu X, *et al.* Impact of patient-specific factors, irradiated left ventricular volume, and treatment set-up errors on the development of myocardial perfusion defects after radiation therapy for left-sided breast cancer. *Int J Radiat Oncol Biol Phys* 2006;66: 1125–1134.
2. Borger JH, Hooning MJ, Boersma LJ, *et al.* Cardiotoxic effects of tangential breast irradiation in early breast cancer patients: The role of irradiated heart volume. *Int J Radiat Oncol Biol Phys* 2007;69: 1131–1138.
3. Ishikura S, Nihei K, Ohtsu A, *et al.* Long-term toxicity after definitive chemoradiotherapy for squamous cell carcinoma of the thoracic esophagus. *J Clin Oncol* 2003;21:2697–2702.
4. Schultz-Hector S, Trott KR. Radiation-induced cardiovascular diseases: Is the epidemiologic evidence compatible with the radiobiologic data? *Int J Radiat Oncol Biol Phys* 2007;67:10–18.
5. Gagliardi G, Constine LS, Moiseenko V, *et al.* Radiation dose-volume effects in the heart. *Int J Radiat Oncol Biol Phys* 2010;76:S77–S85.
6. Darby SC, Cutter DJ, Boerma M, *et al.* Radiation-related heart disease: Current knowledge and future prospects. *Int J Radiat Oncol Biol Phys* 2010;76:656–665.
7. Masci PG, Dymarkowski S, Rademakers FE, *et al.* Determination of regional ejection fraction in patients with myocardial infarction by using merged late gadolinium enhancement and cine MR: Feasibility study. *Radiology* 2009;250:50–60.
8. Kumekawa Y, Kaneko K, Ito H, *et al.* Late toxicity in complete response cases after definitive chemoradiotherapy for esophageal squamous cell carcinoma. *J Gastroenterol* 2006;41:425–432.
9. Morota M, Gomi K, Kozuka T, *et al.* Late toxicity after definitive concurrent chemoradiotherapy for thoracic esophageal carcinoma. *Int J Radiat Oncol Biol Phys* 2009;75:122–128.
10. Mukherjee S, Aston D, Minett M, *et al.* The significance of cardiac doses received during chemoradiation of oesophageal and gastro-oesophageal junctional cancers. *Clin Oncol (R Coll Radiol)* 2003; 15:115–120.

11. Tripp P, Malhotra HK, Javle M, *et al.* Cardiac function after chemoradiation for esophageal cancer: Comparison of heart dose-volume histogram parameters to multiple gated acquisition scan changes. *Dis Esophagus* 2005;18:400–405.
12. Frickhofen N, Beck FJ, Jung B, *et al.* Capecitabine can induce acute coronary syndrome similar to 5-fluorouracil. *Ann Oncol* 2002;13:797–801.
13. Kosmas C, Kallistratos MS, Kopterides P, *et al.* Cardiotoxicity of fluoropyrimidines in different schedules of administration: A prospective study. *J Cancer Res Clin Oncol* 2008;134:75–82.
14. Meinardi MT, Gietema JA, van der Graaf WT, *et al.* Cardiovascular morbidity in long-term survivors of metastatic testicular cancer. *J Clin Oncol* 2000;18:1725–1732.
15. Weijl NI, Rutten MF, Zwinderman AH, *et al.* Thromboembolic events during chemotherapy for germ cell cancer: A cohort study and review of the literature. *J Clin Oncol* 2000;18:2169–2178.
16. Feldman DR, Bosl GJ, Sheinfeld J, *et al.* Medical treatment of advanced testicular cancer. *JAMA* 2008;299:672–684.
17. Torrisi JM, Schwartz LH, Gollub MJ, *et al.* CT findings of chemotherapy-induced toxicity: What radiologists need to know about the clinical and radiologic manifestations of chemotherapy toxicity. *Radiology* 2011;258:41–56.
18. Nellessen U, Zingel M, Hecker H, *et al.* Effects of radiation therapy on myocardial cell integrity and pump function: Which role for cardiac biomarkers? *Chemotherapy* 2010;56:147–152.
19. Heidenreich PA, Hancock SL, Vagelos RH, *et al.* Diastolic dysfunction after mediastinal irradiation. *Am Heart J* 2005;150:977–982.
20. Erven K, Jurcut R, Weltens C, *et al.* Acute radiation effects on cardiac function detected by strain rate imaging in breast cancer patients. *Int J Radiat Oncol Biol Phys* 2011;79:1444–1451.

Jpn J Radiol (2012) 30:340–344
DOI 10.1007/s11604-011-0046-3

CASE REPORT

Successful hyperbaric oxygen therapy for laryngeal radionecrosis after chemoradiotherapy for mesopharyngeal cancer: case report and literature review

Madoka Abe · Yoshiyuki Shioyama · Kotaro Terashima · Mioko Matsuo · Iwao Hara · Satoru Uehara

Received: 17 October 2011 / Accepted: 16 December 2011 / Published online: 19 January 2012

Abstract Laryngeal radionecrosis is one of the most troublesome late complications of radiotherapy, because it is frequently resistant to treatment and laryngectomy is required in the worst case. Here, we report a case of laryngeal radionecrosis, successfully treated by use of hyperbaric oxygen (HBO) therapy, in which laryngectomy was avoided. A 67-year-old male received radical chemoradiotherapy (CRT) for mesopharyngeal cancer, which included radiotherapy with a total dose of 71.4 Gy/38 Fr and chemotherapy with CDDP + S-1. He developed dyspnea and throat pain 9 months after completion of CRT. Laryngoscopy revealed vocal cord impairment because of severe laryngeal edema. He was diagnosed as having laryngeal radionecrosis and initially received conservative therapy combined with antibiotics, steroids, and prostaglandins. Because his dyspnea was persistent despite this treatment, HBO therapy was administered 20 times, and resulted in complete remission of the dyspnea. HBO therapy, therefore, is regarded as an effective conservative therapeutic option for laryngeal radionecrosis.

M. Abe (✉) · K. Terashima · S. Uehara
Department of Radiology, National Hospital Organization Kyushu Cancer Center, 3-1-1 Notame, Minami-ku, Fukuoka 811-1395, Japan
e-mail: abe.m@nk-cc.go.jp

Y. Shioyama
Department of Heavy Particle Therapy and Radiation Oncology, Graduate School of Medical Sciences, Kyushu University, Fukuoka, Japan

M. Matsuo
Department of Head neck Surgery, National Hospital Organization Kyushu Cancer Center, Fukuoka, Japan

I. Hara
Section of Dentistry and Oral Surgery, Keikoukai Hara Hospital, Fukuoka, Japan

Keywords Hyperbaric oxygen therapy · Laryngeal radionecrosis · Mesopharyngeal cancer

Introduction

Chemoradiotherapy (CRT) is an important treatment modality for head and neck cancer with regard to preservation of organ structure and function. It is used widely as the primary treatment for early-stage cancers. Acute adverse effects, for example mucositis, dermatitis, and guttural edema, develop, to different extents, in almost all cases of CRT; usually, however, these are resolved within a few months after the treatment. On the other hand, serious late adverse effects, for example mucosal ulceration of the gingiva, neck fistula, and osteo/chondroradionecrosis, are observed in rare cases. Despite the rarity of these late adverse effects, because of severe and persistent symptoms that are often resistant to treatment patients' quality of life tends to be substantially impaired. Laryngeal radionecrosis is one of the most troublesome late adverse effects, because laryngectomy is sometimes inevitable in severe cases. Hyperbaric oxygen (HBO) therapy is a standard adjuvant treatment modality for mandibular osteoradionecrosis (ORN) [1]. However, reports of its use to treat laryngeal radionecrosis are limited and a treatment procedure has not yet been established [2]. Here, we report a case of laryngeal radionecrosis successfully treated with HBO therapy.

Case report

A 67-year-old male received CRT for mesopharyngeal cancer (left lateral wall, cT2N2bM0) as initial treatment at our department from May to June 2010. Radiotherapy with

a total dose of 71.4 Gy/38 Fr using 4 MV X-ray was performed in combination with chemotherapy using cisplatin and S-1. Of the 71.4 Gy the patient received, 41.4 Gy was irradiated in 23 fractions on the initial field including the whole neck and supraclavicular region. 30 Gy was then boosted in 15 fractions on a field fitted to the primary tumor and metastatic lymph nodes. The estimated dose to the larynx was 95–100% of the prescribed dose and no hot spot was detected in the larynx (Fig. 1). During the first 5 days of radiotherapy, 20 mg/m^2 CDDP was administered to the patient as the first *kur* (total amount 160 mg). However, this chemotherapy regimen had to be changed to 80 mg/day of S-1 because of renal failure, and S-1 was administered for 14 days instead of the second *kur* of CDDP (total amount of 1120 mg). The initial responses of the primary site and cervical lymph node metastases were complete response and partial response, respectively. Therefore, left radical neck dissection was performed 1 month after completion of CRT. The patient complained of throat pain and hoarseness, and laryngoscopy revealed marked mucositis on the treatment site and laryngeal edema at the time of CRT completion. However, all of these symptoms resolved within 1 month, with laryngoscopy confirming the resolution of mucositis. Laryngeal edema, on the other hand, was still observed 6 months later.

Nine months after CRT, he revisited our hospital, complaining of dyspnea and throat pain. He presented stridor with the oxygen saturation (SpO_2) of 97–98% at room air. Laryngoscopy revealed severe mucositis of the larynx and meso-hypopharynx. In addition, the glottis could not be seen clearly, because of marked laryngeal edema, and the right and left vocal cords appeared to be fixed and impaired, respectively (Fig. 2). Therefore, he was diagnosed with grade III laryngeal radionecrosis based on Chandler's classification (Table 1) [3] and was admitted to the hospital as an emergency. Medical interview revealed no history of alcohol consumption, smoking, use of steroids, or tooth extraction during or after CRT, all of which can trigger radionecrosis. Computerized tomography (CT) scan on the same day revealed an obvious low-density area indicative of severe edema in meso-hypopharynx and larynx. In addition, the thyroid cartilage and the arytenoids cartilages were found to be fragmented and collapsed (Fig. 2). Conservative therapy, initiated immediately upon admission, included antibiotics, steroids, and prostaglandins, combined with other supportive care, for example steam inhalation and nutrition support. The amount of administered steroids was reduced from 200 mg predonine to 10 mg in 3 weeks, and antibiotics and prostaglandins were administered intravenously for the initial 2 weeks, and then orally. Although this treatment resolved the stridor and throat pain, dyspnea persisted even after 3 weeks of this therapy. Laryngoscopy found some improvement of laryngeal edema but the right vocal cord was found still fixed. Therefore, the patient was transferred to another hospital to receive HBO therapy. HBO therapy was

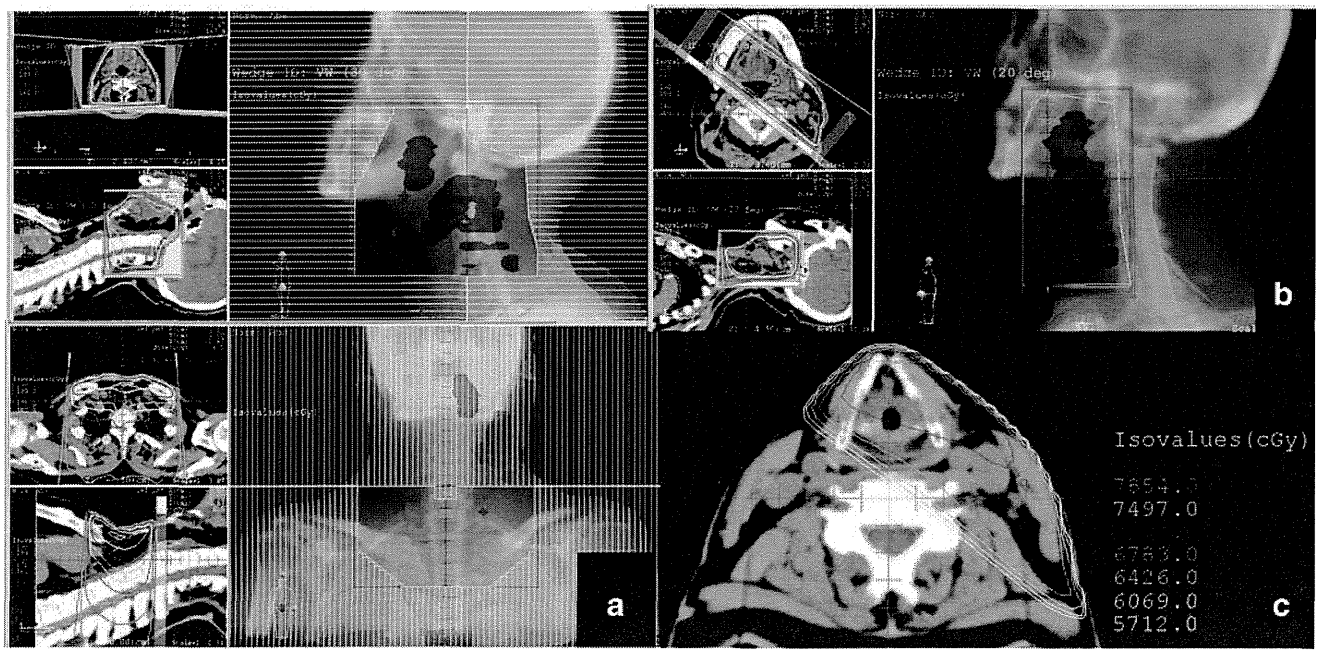

Fig. 1 **a** Initial planning of radiotherapy: bilateral neck and supraclavicular region were irradiated, using the half-beam method. **b** Boost planning of radiotherapy: oblique opposed beams were set to boost a field which fitted the primary tumor and lymph node metastases. **c** Section of the larynx at CT planning: the larynx was covered by the 95% line (*orange line*) of the prescribed dose. No hot spot was observed in the larynx

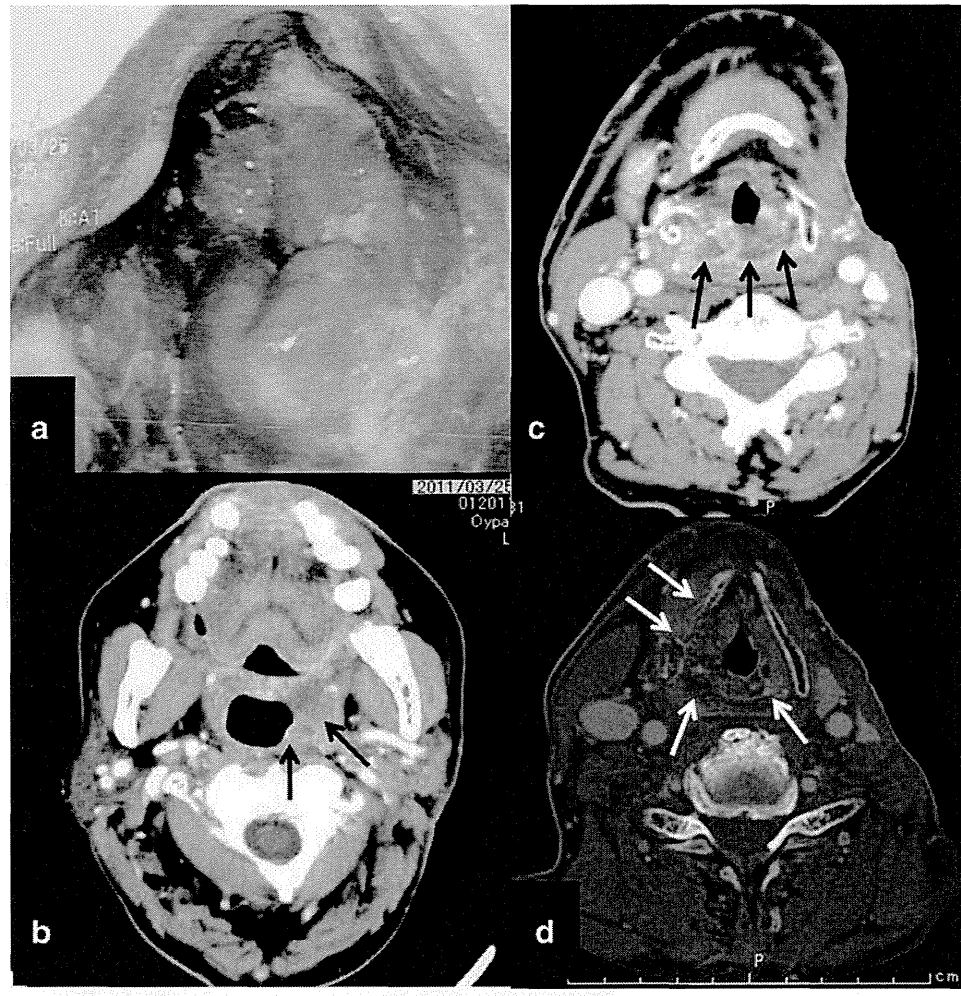

Fig. 2 **a** Laryngoscopy 6 months after completion of chemoradiotherapy: marked mucositis of the larynx is revealed. The glottis is hardly visible because of severe edema. **b–d** CT scan on the same day as laryngoscopic examination: the low-density area indicative of severe edema has expanded into the meso-hypopharynx and larynx (*black arrows*). The shapes of the thyroid cartilage and the arytenoids cartilages are obscure and fragmented (*white arrows*), implying chondronecrosis

Table 1 Chandler's classification for laryngeal necrosis (from Ref. [3])

Grade	Symptoms	Signs
I	Slight hoarseness	Slight edema, telangiectasia
	Slight mucosal dryness	
II	Moderate hoarseness	Slight impairment of cord motility, moderate edema and erythema
	Moderate mucosal edema	
III	Severe hoarseness with dyspnea	Severe impairment of cord motility or fixation of one vocal cord
	Moderate odynophagia and dysphagia	Marked edema, skin changes
IV	Respiratory distress, severe pain	Fistula, fetor oris
		Fixation of skin to larynx
	Severe odynophagia, weight loss	Laryngeal obstruction and edema occluding airway, fever
	Dehydration	

performed daily at 2 atmospheres absolute (ATA) with 100% oxygen for 1 h each. After 20 sessions of HBO therapy, his dyspnea completely resolved, and movement of the vocal cords was confirmed by laryngoscopy, recovering to normal. The CT scan also revealed marked shrinkage of the low-density area with the shapes of the cartilages obviously becoming well defined, implying improvement of the radionecrosis (Fig. 3). Furthermore, laryngoscopy performed at subsequent monthly check-ups revealed gradual improvement of laryngeal edema and no recurrence of cancer.

Discussion

Chandler classified radiation-induced laryngeal injury into four stages according to clinical findings and symptoms (Table 1) [3]. This system is very useful and widely used for establishing guidelines for therapy. Chandler's grade III and IV are regarded as "radionecrosis" by clinical consensus, although pathological evidence is lacking. The reported incidence of laryngeal radionecrosis after radical radiotherapy has been less than 1% since the 1990s. Although typical occurrence of laryngeal necrosis is

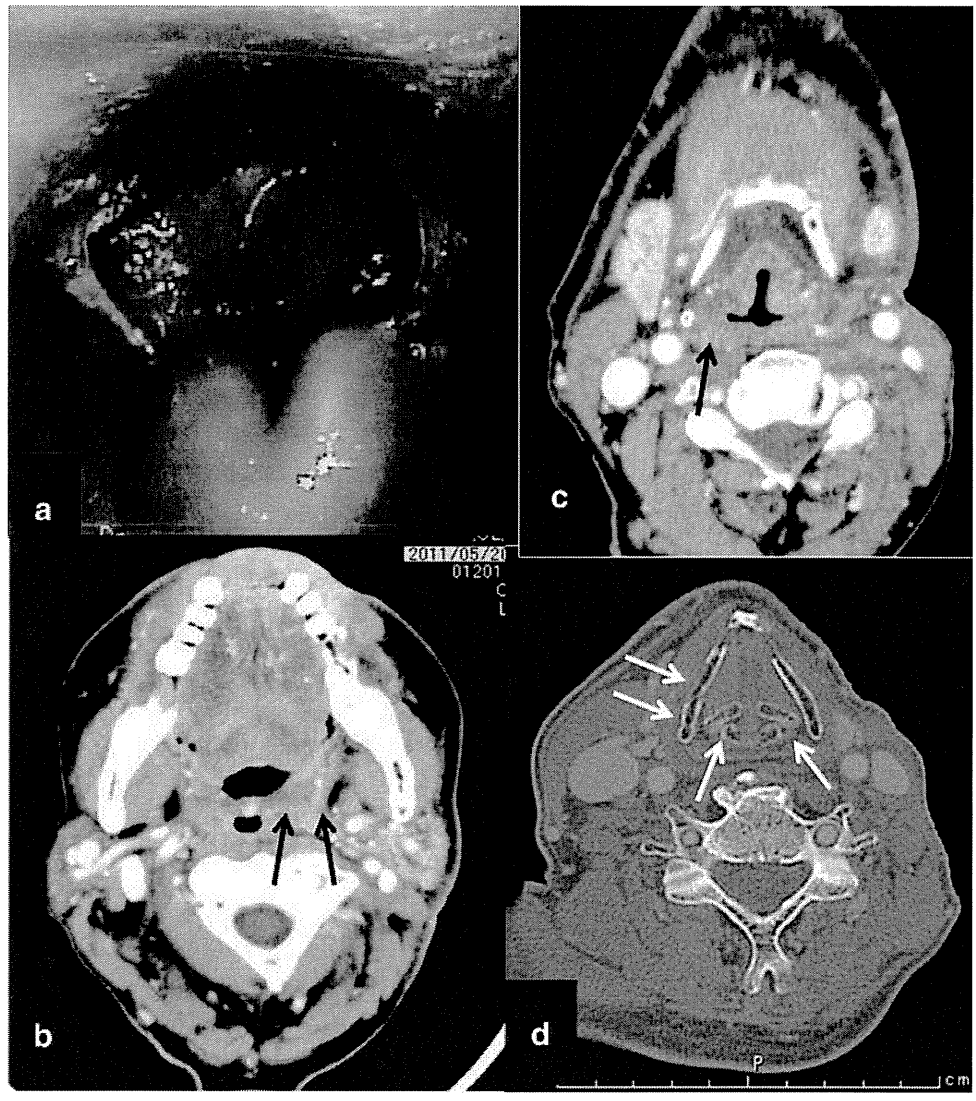

Fig. 3 **a** Laryngoscopy after 20 sessions of HBO therapy: mucositis is obviously resolved and edema is slightly improved. **b–d** CT scan after 20 sessions of HBO therapy: the low-density area has become almost negligible (*black arrows*). The shapes of cartilages are more defined and fragmentation is not observed (*white arrows*)

accompanied by predisposing factors, for example continuous smoking and alcohol consumption, diabetes, steroid use, infection, and local tumor recurrence after radiotherapy [2], the patient in our case had no such history. Because neck dissection can induce hypoxic conditions in the larynx, this could have been the trigger of radionecrosis in our case. However, this remains speculative, because no complication was observed after neck dissection and a definitive causal relationship cannot be drawn.

Initial standard treatment for laryngeal radionecrosis is conservative therapy including steam inhalation, nutrition support, antibiotics, steroids, and, in recent times, prostaglandins. When a patient does not respond well to these treatments, HBO therapy and surgical intervention are considered as the next step. Hypoxia, hypocellularity, and hypovascularity due to irradiation have been thought of as the main causes of radionecrosis, although its mechanism of pathogenesis has not been fully elucidated [1]. HBO therapy is regarded as an effective means of rescuing such conditions, because it stimulates angiogenesis, fibroblast and osteoblast proliferation, and collagen formation in irradiated tissues. HBO therapy has been used for management of ORN, particularly mandibular ORN, since the 1960s [4]. Marx established the procedure for HBO therapy combined with surgery for ORN in 1983 [1]; this has become the standard adjuvant treatment for ORN. On the other hand, reports of HBO therapy for laryngeal radionecrosis are limited and a treatment procedure has not yet been established. In 2000 Filntisis et al. [2] reported 18 cases treated with HBO therapy and conducted a literature review of 25 cases. However, few reports have been published since then [5–9]. The cases reported previously were all of Chandler's grade III/IV laryngeal radionecrosis and received radiotherapy of 45–86 Gy. HBO regimens varied from 2.0 to 2.5 ATA for 60–120 min with the number of treatment sessions ranging from 6 to 80 (Table 2). In such

Table 2 Summary of the published literature on HBO therapy for laryngeal radionecrosis (from Refs. [2, 5–9])

Authors	Number of patients	Chandler's classification	Chemoradiotherapy	HBO therapy (ATA × min × numbers)	Outcome
Hart et al. [2]	5	IV	RTx; N/A CTx; N/A	2 × 120 × 60	4 improved, 1 failed
Farmer et al. [2]	1	IV	RTx; N/A CTx; N/A	2 × 120 × 40	Improved
Davis et al. [2]	1	IV	RTx; N/A CTx; N/A	2.4 × 90 × 60	Improved
Strauss [2]	1	IV	RTx; N/A CTx; N/A	N/A × N/A × 20	Failed
Ferguson et al. [2]	8	III/IV	RTx; 60–70 Gy CTx; N/A	2 × 120 × 39–76 (49)	7 improved, 1 failed
Feldmeier et al. [2]	9	III/IV	RTx; 45–70 Gy CTx; N/A	2.4 × 90 × 8–41 (28)	All improved
Filntisis et al. [2]	18	III/IV	RTx; 50–75.45 Gy CTx; N/A	2 × 120 × 6–80 (43)	13 improved, 5 failed
Hsu et al. [5]	1	IV	RTx; 60 Gy CTx; −	2 × 60 × 40	Improved
Nishida et al. [8]	1	IV	RTx; 64.8 Gy CTx; +	2 × 120 × 20	Improved
Matsushita et al. [9]	2	IV	RTx; 79.3–80 Gy CTx; +	2.5 × 60 × N/A	All improved
Narozny et al. [6]	6	III/IV	RTx; 60–86 Gy CTx; N/A	2.5 × 60 × 8–20 (16)	All improved
Scott et al. [7]	5	III/IV	RTx; 66.6–70 Gy CTx; N/A	2.5 × 90 × 15–25	4 improved, 1 N/A

RTx radiotherapy, *CTx* chemotherapy, *N/A* not available

reports, the therapy regimen largely depended on each hospital's guideline and the number of treatments was usually determined by clinicians, on the basis of the patient's clinical symptoms. The effectiveness of HBO therapy was estimated to be 86% overall, with all of the successful cases avoiding laryngectomies. Interestingly, all of Chandler's grade III cases responded well to the treatment, indicating the importance of early HBO intervention.

Regarding the adverse effects of HBO therapy, the previous studies reported several cases in which myopia and otalgia developed as manifestations of barotraumas, necessitating myringotomies. However, these symptoms resolved quickly, and no severe HBO complications, for example pulmonary injury and seizure activity, were reported [2, 7–9]. In addition to adverse effects, recurrent tumor acceleration induced by HBO therapy may be another concern. However, there has been no convincing evidence that HBO therapy stimulates tumor growth; previous literature and our case revealed no definite cancer growth enhancement as a result of HBO therapy [2, 5–9].

In conclusion, HBO therapy is an effective treatment option and should be considered, in combination with other conservative therapy, for laryngeal radionecrosis, especially in the situation of increased availability of HBO facilities in recent years.

References

1. Marx RE. A new concept in the treatment of osteoradionecrosis. J Oral Maxillofac Surg. 1983;41:351–7.
2. Filntisis GA, Moon RE, Kraft KL, Farmer JC, Scher RL, Piantadosi CP. Laryngeal radionecrosis and hyperbaric oxygen therapy: report of 18 cases and review of the literature. Ann Otol Rhinol Laryngol. 2000;109:554–62.
3. Chandler JR. Radiation fibrosis and necrosis of the larynx. Ann Otol Rhinol Laryngol. 1979;88:509–14.
4. Pasquier D, Holesher T, Schmutz J, Dische S, Mathieu D, Baumann M, et al. Hyperbaric oxygen therapy in the treatment of radio-induced lesions in normal tissues: a literature review. Radiother Oncol. 2004;72:1–13.
5. Hsu YC, Lee KW, Ho KY, Tsai KB, Kuo WR, Wang LF, et al. Treatment of laryngeal radionecrosis with hyperbaric oxygen therapy: a case report. Kaohsiung J Med Sci. 2005;21:88–92.
6. Narozny W, Sicko Z, Kot J, Stankiewicz C, Przewozny T, Kuczkowski J. Hyperbaric oxygen therapy in the treatment of complications of irradiation in head and neck area. UHM. 2005;32:103–10.
7. London SD, Park SS, Gampper TJ, Hoard MA. Hyperbaric oxygen for the management of radionecrosis of bone and cartilage. Laryngoscope. 1998;108:1291–6.
8. Nishida A, Honda N, Kitani Y, Tsujimura M, Adachi T, Fujiki N, et al. Treatment of laryngeal radionecrosis with hyperbaric oxygen therapy: a case report. Jibirinshou. 2007;100:1021–6.
9. Matsushita H, Nemoto K, Ogawa Y, Ariga H, Takeda K, Sakayauchi T, et al. Effects of hyperbaric oxygen therapy (HBO) on radiation-induced late sequelae. J Jpn Soc Ther Radiol Oncol. 2007;19:147–55.

Journal of Radiation Research, 2012, 53, 961–972
doi: 10.1093/jrr/rrs043 Advance Access Publication 26 July 2012

Computerized estimation of patient setup errors in portal images based on localized pelvic templates for prostate cancer radiotherapy

Hidetaka ARIMURA[1,*], Wataru ITANO[2], Yoshiyuki SHIOYAMA[3], Norimasa MATSUSHITA[2], Taiki MAGOME[2], Tadamasa YOSHITAKE[3], Shigeo ANAI[4], Katsumasa NAKAMURA[5], Satoshi YOSHIDOME[4], Akihiko YAMAGAMI[6], Hiroshi HONDA[5], Masafumi OHKI[1], Fukai TOYOFUKU[1] and Hideki HIRATA[1]

[1]Department of Health Sciences, Faculty of Medical Sciences, Kyushu University, Japan
[2]Department of Health Sciences, Graduate School of Medical Sciences, Kyushu University, Japan
[3]Department of Heavy Particle Therapy and Radiation Oncology, Graduate School of Medical Sciences, Kyushu University, Fukuoka, Japan
[4]Department of Radiology, Kyushu University Beppu Hospital, Japan
[5]Department of Clinical Radiology, Graduate School of Medical Sciences, Kyushu University, Fukuoka, Japan
[6]Jyunwakai Memorial Hospital, Miyazaki, Japan
*Corresponding author: Division of Quantum Radiation Science, Department of Health Sciences, Faculty of Medical Sciences, Kyushu University 3-1-1, Maidashi, Higashi-ku, Fukuoka 812-8582, Japan; Email: arimurah@med.kyushu-u.ac.jp

(Received 31 January 2012; revised 14 May 2012)

We have developed a computerized method for estimating patient setup errors in portal images based on localized pelvic templates for prostate cancer radiotherapy. The patient setup errors were estimated based on a template-matching technique that compared the portal image and a localized pelvic template image with a clinical target volume produced from a digitally reconstructed radiography (DRR) image of each patient. We evaluated the proposed method by calculating the residual error between the patient setup error obtained by the proposed method and the gold standard setup error determined by consensus between two radiation oncologists. Eleven training cases with prostate cancer were used for development of the proposed method, and then we applied the method to 10 test cases as a validation test. As a result, the residual errors in the anterior–posterior, superior–inferior and left–right directions were smaller than 2 mm for the validation test. The mean residual error was 2.65 ± 1.21 mm in the Euclidean distance for training cases, and 3.10 ± 1.49 mm for the validation test. There was no statistically significant difference in the residual error between the test for training cases and the validation test ($P = 0.438$). The proposed method appears to be robust for detecting patient setup error in the treatment of prostate cancer radiotherapy.

Keywords: Computerized method; patient setup error; prostate cancer; portal image; digitally reconstructed radiography; template matching technique

INTRODUCTION

The incidence of prostate cancer has increased throughout the world, even in Japan [1] and other Asian countries that historically have had a low incidence of prostate cancer. This trend has led to a growing number of patients receiving radiation therapy as a definitive treatment for prostate cancer. Recently, high-precision radiotherapies such as conformal radiotherapy (CRT) and intensity-modulated radiation therapy (IMRT) have been routinely employed for dose escalation to the whole prostate and/or reduction of rectal toxicity [2]. Accurate patient setup is essential in high-precision radiotherapy for prostate cancer, because deviations in the delivered beam geometry may result in decreased tumor control and increased complications in the surrounding normal tissue. However, the majority of clinical facilities do not have an automatic setup system, and thus the radiation oncologists or radiological technologists

have to verify the patient setup during the radiation treatment by subjective visual comparison between a portal image and a digitally reconstructed radiograph (DRR) produced in treatment planning, without any objective data on the setup errors, which are estimated by an independent method. In addition, even in facilities that have an automatic setup system, the patient setup error correction function does not always work well in an actual clinical setting, and thus a manual setup is often carried out after the automatic one. In such cases, experienced radiation oncologists can make a reproducible correction of the patient setup errors within a short period of time, but less experienced oncologists may not achieve the same performance. To resolve this issue, we here developed a computer-assisted radiotherapy system that can provide radiation oncologists with the objective data that are needed for correcting patient setup errors.

Many automated or semi-automated methods for estimation of patient setup errors have been studied based on two-dimensional (2D) or three-dimensional (3D) registration [3–10]. There are two types of patient setup methods based on registrations between two types of images, that is, 2D/2D and 3D/3D registrations. For 2D/2D registration, the 2D portal image and the 2D DRR image derived from a planning kV-3D computed tomography (CT) image or pre-treatment kV- or MV-3D CT image can be used [4, 5, 7, 8]. On the other hand, in 3D/3D registration, the planning kV-3D CT image can be registered with the pre-treatment kV- or MV-3D CT image [3, 6–10]. In conventional methods, the patient setups are performed by using registrations based on whole images including bony anatomical structures and soft tissue around the prostate. However, the displacements of the prostate and its surrounding anatomical structures could be independent of each other [11]. For that reason, radiation oncologists are likely to choose the localized anatomical structures closer to the prostate as reference points for estimation of setup errors. In addition, Morishita *et al.* [12] reported that localized anatomical templates that included the thoracic field, cardiac shadows, the superior mediastinum, lung apices, a part of the right lung and the right lower lung were useful for patient recognition in the picture archiving and communication system (PACS) environment. Therefore, based on the habits of radiation oncologists during clinical setup and the results of Morishita *et al.*, we considered that localized anatomical templates extracted from pelvic regions close to the prostate in the DRR image could feasibly be used for identifying the irradiation center in the portal image; these templates have not previously been studied for the estimation of patient setup errors. The purpose of this study was to develop a computerized method for estimating patient setup errors in portal images based on localized pelvic templates, including a clinical target volume for prostate cancer radiotherapy.

MATERIALS AND METHODS

Figure 1 shows an illustration of the overall scheme of the proposed method for estimation of patient setup errors in portal images, which mainly consisted of the following four steps.

(i) determination of an actual center of an irradiation field in the portal image;
(ii) extraction of a localized pelvic template with a prostate region of each patient using a mean pelvic template and four anatomical feature templates;
(iii) detection of a planned center in the portal image based on a technique for matching the portal image with the localized pelvic template;
(iv) estimation of the patient setup error by calculating the difference between the actual and planned centers in the portal image.

Clinical cases

This study was performed under a protocol approved by the institutional review board of the Kyushu University hospital. A training data set of 11 patients (ages: 60–84 years; median: 71 years) with prostate cancer, who received CRT through 2009, was selected for development of the proposed method. A total dose of 72 Gy in 36 fractions (2 Gy per fraction) was delivered for all patients during the

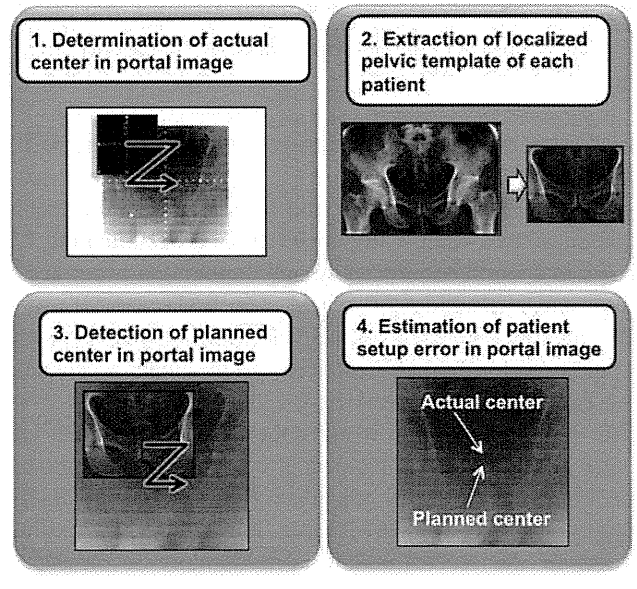

Fig. 1. An illustration of the overall scheme of our proposed method for estimating patient setup error in a portal image based on a localized pelvic template of an individual patient undergoing prostate cancer radiotherapy. The patient setup error was estimated by calculating the difference between the actual and planned centers in the portal image.

treatment course. The planning 3D CT images and the portal images for the 11 patients were used for development of the proposed method. All patients were scanned to acquire planning CT images using a four-slice CT scanner (Mx 8000; Philips, Einthoven, NL) with a slice thickness of 3.0 mm. The pixel sizes of the planning CT images were 0.78 mm ($n=2$), 0.82 mm ($n=1$), 0.86 mm ($n=2$), 0.88 mm ($n=4$) and 0.98 mm ($n=2$). The radiation treatment protocols were performed on an Eclipse treatment planning system (Varian Medical Systems Inc., Palo Alto, CA, USA). The portal images (matrix size: 512×384; pixel size: 0.56 mm; stored bits: 16) used for verification of patient setup prior to actual radiation delivery were acquired using 4- or 6-MV X-ray beams with a linear accelerator (Clinac 21 EX; Varian Medical Systems Inc.) that was equipped with an electronic portal imaging device (EPID) (AS-500; Varian Medical Systems Inc.). We selected eight portal images of eight patients at the last treatment time, and six portal images of three patients at two treatment times including the last one. The source-to-axis distance (SAD) and source-to-image receptor distance (SID) were 100 cm and 140 cm, respectively. Orthogonal portal images in the anterior–posterior (AP) (0°) and lateral projections (270°) were obtained to compare them with the corresponding planning DRRs.

A test data set of 10 prostate patients (ages: 64–79 years; median: 74.5 years) was selected for a validation test of the proposed method. There was no statistically significant difference in age between the training and test groups ($P=0.48$). The pixel sizes of the test planning CT images were 0.78 mm ($n=2$), 0.88 mm ($n=6$), 0.98 mm ($n=1$) and 0.90 mm ($n=1$).

Reconstruction of DRR images from planning CT images

The DRR images in the AP and lateral views were reconstructed as two beam's eye views from a 3D planning CT image in a world coordinate system including a linear accelerator and a planning CT image. The SAD and SID were 100 cm and 140 cm, respectively, which was the same geometry as for the EPID mounted on the linear accelerator. The isocenter in the planning CT image was placed at an SAD of 100 cm in the world coordinate system. The isocenter coordinate was obtained in a file of digital imaging and communications in medicine (DICOM) for radiation therapy, that is, a DICOM-RT file. Figure 2 shows an illustration of the reconstruction of a digitally reconstructed radiography (DRR) image from a planning CT image based on a ray casting method [13], where sampling points are obtained on a ray. For reconstruction of the DRR image, a divergent primary beam with a number of rays produced from an X-ray focal spot of the linear accelerator was virtually delivered to a 3D CT image. Then, CT values on each ray in the divergent beam in the 3D CT image were

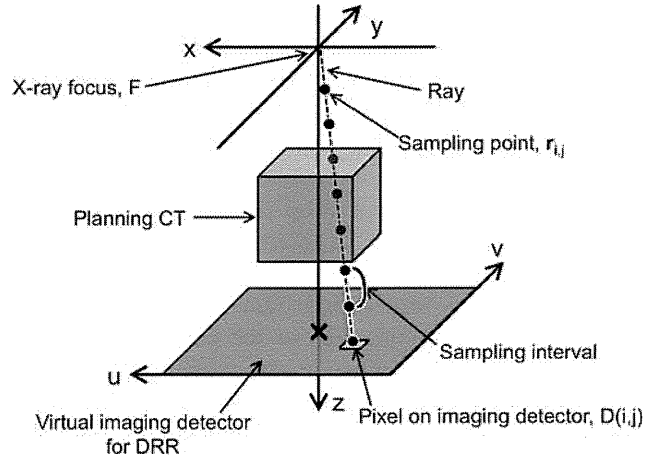

Fig. 2. An illustration of the reconstruction of a digitally reconstructed radiography (DRR) image from a planning CT image based on a ray casting method [13], where sampling points are obtained on a ray.

sampled at a certain interval and accumulated for each pixel in a virtual imaging plane, which had the same pixel size as the EPID (0.56 mm), but a 512×512 matrix size. The DRR image was reconstructed by the following equation:

$$D(i,j)=\sum_{n=1}^{N(i,j)} f\left(\mathbf{r}_n(i,j)\right) \quad (1)$$

where $D(i, j)$ is the pixel value on a virtual imaging detector for production of the DRR image, f is the planning CT image, $\mathbf{r}_n(i, j)$ is the nth sampling position vector on a ray from a pixel, $P(i, j)$, on the imaging detector to an X-ray focus, F, which was used for sampling CT values, and $N(i, j)$ is the number of the sampling data points for a pixel (i, j). The CT values on the ray were interpolated by using a cubic interpolation technique, because the coordinate of the sampling position on the ray was not always an integer but was always a real number.

Production of a mean pelvic template and anatomical feature templates

A localized pelvic template including a prostate region, which was used for detection of a planned center in the portal image, was extracted from the DRR image for each patient using a mean pelvic template and the four anatomical feature templates described below. A mean pelvic template image was produced from five training DRR images by registering all cases to one reference case by using an affine transformation with the anatomical feature points. Five training images with a typical bony pelvis in terms of size and shape were manually selected for producing the mean pelvic template image from the 11 training images used in this study, because the anatomical feature points used for production of localized pelvic templates were not accurately detected by the mean pelvic template and anatomical feature templates including atypical cases.

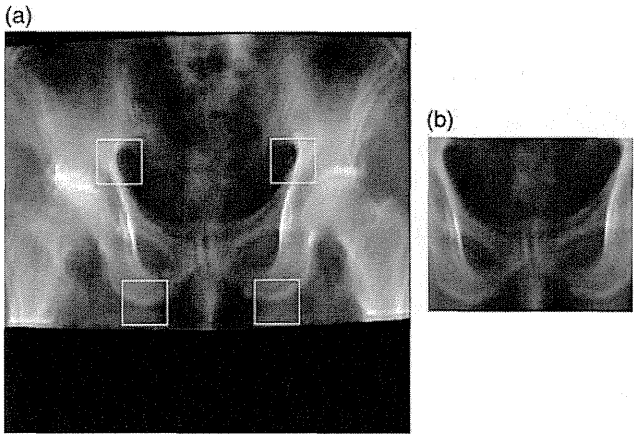

Fig. 3. (**a**) A mean DRR image in the anterior-posterior view, and (**b**) a mean pelvic template image. The white lines in Fig. 3a indicate four anatomical feature template regions.

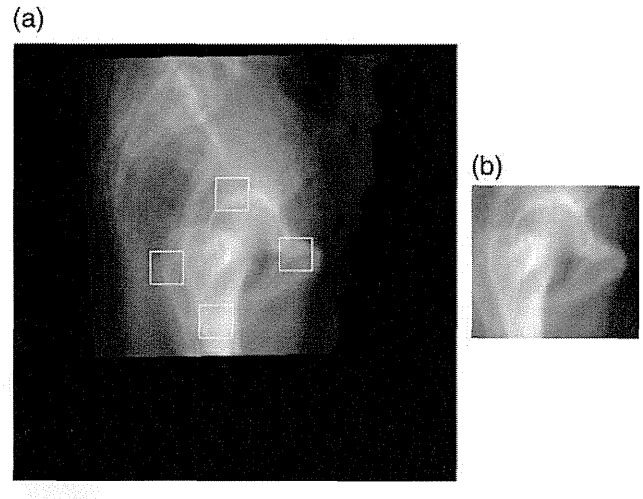

Fig. 4. (**a**) A mean DRR image in the lateral view, and (**b**) a mean pelvic template image. The white lines in Fig. 4a indicate four anatomical feature template regions.

In the clinical setting, the patient setup is usually performed based on anatomical characteristic bony structures around the prostate. Because the difference in movement between the prostate and the more distant bony structures can be large, radiation oncologists tend to select the localized bony structures closer to the prostate as anatomical feature points for estimating patient setup errors. Therefore, we manually selected the left and right lower ends of the ischial bone, and left and right ends of the foramen ischiadicum majora as four anatomical feature points in the AP view of the DRR image for the registration. The rectangular region, which was determined by the four feature points, included a prostate region. On the other hand, the four feature points in the lateral view were the apex of the symphysis pubis, acetabular upper end, inferior pubic ramus and back side of the upper end of the femur in the lateral view. Finally, the pelvic region in the mean DRR image was cropped as mean pelvic templates so that the four anatomical feature points could be included. Figure 3a and b shows a mean DRR image in the AP view, and a mean pelvic template image extracted from the mean DRR image, respectively, and Figure 4a and b show those in the lateral view.

Four anatomical feature templates of the corresponding anatomical regions mentioned above were extracted by a certain square region from the mean pelvic DRR images in the AP and lateral views, respectively. The template matrix size was empirically determined as 23 mm × 23 mm (41 × 41) pixels in this study. Figures 3a and 4a also show four regions (white lines) corresponding to the anatomical feature templates.

Estimation of the patient setup error

Determination of the actual center of an irradiation field in a portal image

The actual center in an irradiation field on the portal image was determined by searching a measuring scale within the irradiation field in the portal image using a template-matching technique based on the cross-correlation coefficient (CC). However, determination of the actual center of an irradiation field in a portal image depends on the individual institution, the imaging system used and whether or not the system includes an EPID. For example, the actual centers of the irradiation field in the portal image were determined by using hardware such as a measuring scale in some systems, including the system at our institution, but in other systems, the actual centers are identified using software. Therefore, the details of the method used to determine the actual center in an irradiation field on the portal image are described in Appendix A, because the method has not yet been standardized.

Extraction of a localized pelvic template of each patient

A localized pelvic DRR template of each patient in AP or lateral view was automatically extracted from his own DRR image by cropping a rectangular region, which was determined by using the mean pelvic template and four anatomical feature points. First, the mean pelvic template was registered with a DRR image of each patient by using the template-matching technique while maximizing a CC. The template matching was carried out within a radius of 1.0 cm from the isocenter in the DRR image. Next, each anatomical feature template was registered with its corresponding similar anatomical region within a radius of 1.0 cm from the original position in the mean pelvic template. Then, the localized pelvic template was extracted as a rectangular region determined with the minimum and maximum coordinates of the centers of four anatomical feature templates. Figure 5a, b and c shows a DRR image of a patient, its corresponding Sobel-filtered image (green)

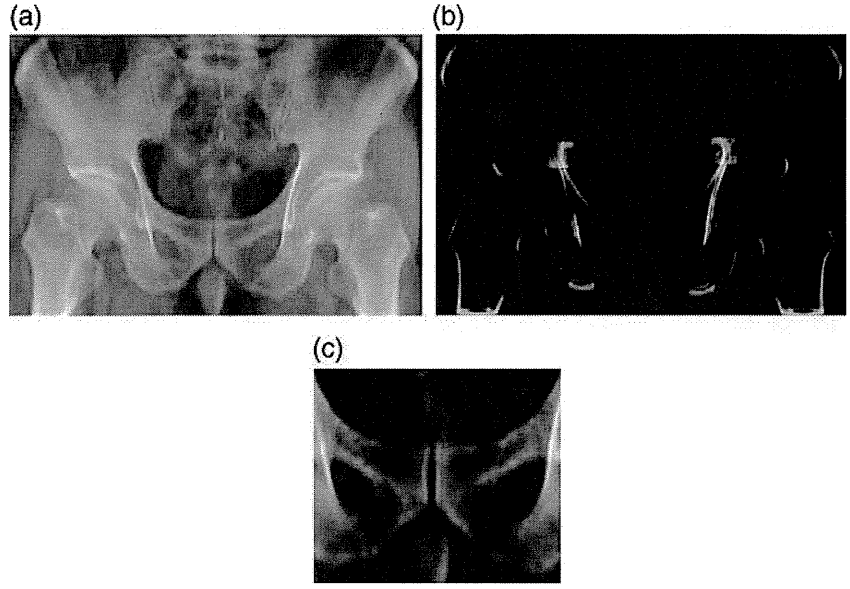

Fig. 5. (**a**) An original DRR image of a patient, (**b**) the corresponding Sobel-filtered image (green) with four feature regions (pink) detected by the anatomical feature templates and (**c**) a localized pelvic template of the same patient.

with four feature regions (pink) detected by the anatomical feature templates, and a localized pelvic template of the patient, respectively. Note that the size of the localized pelvic template shown in Fig. 5c is 80% of the size of the original pelvic template, which was automatically obtained from the patient's own DRR image by using the proposed method explained in this section. Because we investigated the effect of enhancement of bony anatomical structures on the overall performance of the proposed method, the localized pelvic template images with enhancement of bony structures by a Sobel filter were also produced for the estimation of patient setup errors.

Detection of the planned center in a portal image

The planned center in the irradiation field in a portal image was detected using the following two steps: (i) reduction of scale points on the portal image; and (ii) detection of the planned center based on a template-matching technique between the portal image and the localized pelvic template obtained as described in the previous section.

Although a measuring scale is needed to verify the center of the portal image and compare it with the planned isocenter of the planning DRR image in clinical practice, the measuring scale points should be reduced for more accurate template matching between the portal image and the localized pelvic template image. Therefore, the measuring scale points were reduced by inpainting each scale point with a mean filter and a measuring scale binary template. However, since the method seemed to be specific only when the measuring scale was used, the details of the method are illustrated in Appendix B.

The planned center in the irradiation field in the portal image was detected by performing a template matching between the localized pelvic template and the portal image. The planned center (x_{pc}, y_{pc}) of the irradiation field was determined by finding a location with the maximum similarity measure S (x, y) between the portal image I (x, y) and the template image T (x, y) based on the following equation:

$$(x_{pc}, y_{pc}) = \arg\max_{x,y}(S(x,y)). \quad (2)$$

In this template matching, we investigated the effects of the following three parameters on the performance of the proposed method: (i) the optimum size of the localized pelvic template; (ii) similarity measures, that is, the CC and mutual information (MI); and (iii) the enhancement of bony anatomical structures, which are described in 'Evaluation of the proposed method'.

Calculation of patient setup error

The patient setup error was estimated as the distance between the actual center and planned center in the irradiation field of the portal image in the AP, SI and (LR) directions and the 3D Euclidean distance.

Evaluation of the proposed method

The residual error [9] between the patient setup errors obtained by the proposed method and gold standard setup errors obtained by the radiation oncologists was calculated for evaluation of the proposed method. The gold standards for the setup errors were determined based on a consensus

between two experienced radiation oncologists in this study. However, note that we did not investigate the inter-observer variability and intra-observer variability of the gold standards of patient setup errors. The residual error denotes the differences between the patient setup errors obtained by the proposed method and the gold standard patient setup errors. Residual error was calculated in the AP, SI and LR directions and for the Euclidean distance. The residual error of the 3D Euclidean distance was employed for evaluation of the overall performance of the proposed method.

We applied the proposed method to the training data set of 11 prostate patients, that is, a resubstitution test, as well as to the test data set of 10 prostate patients, which was not used for development of the proposed method, that is, a validation test.

To find the optimum parameters for use in the proposed method, we investigated the effects of the following three parameters on the performance of the method: (i) the optimum size of the localized pelvic template; (ii) similarity measures, that is, the CC and MI; and (iii) the enhancement of bony anatomical structures.

Optimum size of the localized pelvic template

In a majority of image-guided radiotherapy systems, the patient setups are performed by using registrations based on whole anatomical structures including soft tissue around the prostate. However, since the prostate and its surrounding anatomical structures can displace independently of each other [11], radiation oncologists are likely to adopt the anatomical structures closer to the prostate (e.g. the pubic symphysis) as reference points. Therefore, the optimum size of the localized pelvic template was investigated by reducing the localized pelvic template size determined in the previous section from 100% to 40% relative size. We defined the 100% relative size for the localized pelvic template as the size of the original pelvic template, which was automatically obtained from the patient's own DRR image by using the method described in the previous section.

Similarity measures

In general, since the accuracy of the registration or template-matching technique in this study depends on the similarity measure, the detection accuracy of the planned center in the irradiation field may change with the similarity measure. In addition, according to a study of Wu *et al.* [14], the robust similarity measures in the patient setup using a registration technique were a normalized CC and normalized MI. Therefore, we evaluated the performance of the proposed method with two similarity measures, that is, the CC and MI, which are widely used for registration in radiological fields.

The CC between the portal image $I(x, y)$ and the template image $T(x, y)$ was based on the following equation [15, 16]:

$$C(x',y') = \frac{1}{X \cdot Y} \sum_{x=0}^{X-1} \sum_{y=0}^{Y-1} \frac{(I(x,y) - \bar{I})(T(x,y) - \bar{T})}{\sigma_i \cdot \sigma_t} \quad (3)$$

where x and y are the coordinates in the image within the overlapped area between the portal and template images, x' and y' are the center coordinates of the template image, $I(x, y)$ is the pixel value at (x, y) in the portal image, $T(x, y)$ is the pixel value at (x, y) in the template image, $\bar{I}$ and σ_i are the mean and the standard deviation of the pixel values of the portal image, respectively, $\bar{T}$ and σ_t are the mean and the standard deviation of the pixel values of the template image within the same overlapped area, respectively, and X and Y are the numbers of pixels in x and y widths of the template image, respectively.

The mutual information at the center coordinate (x', y') between the template image and the portal image was calculated from the following equation [17]:

$$M(x',y') = \sum_{a=0}^{L-1} \sum_{b=0}^{L-1} P_{it}(a,b) \log_2 \frac{P_n(a,b)}{P_i(a)P_t(b)} \quad (4)$$

$$P_{it}(a,b) = \frac{h(a,b)}{X \cdot Y} \quad (5)$$

$$P_i(a) = \sum_{b=0}^{L-1} P_{it}(a,b) \quad (6)$$

$$P_t(b) = \sum_{a=0}^{L-1} P_{it}(a,b) \quad (7)$$

where L is the number of quantization levels; $P_i(a)$ is the probability that the intensity at a pixel in the portal image is a; $P_t(b)$ is the probability that the intensity at a pixel in the template image is b; $P_{it}(a, b)$ is the joint probability that the intensity at a pixel in the portal image is a in conjunction with the event that the intensity at a pixel in the template image is b; $h(a, b)$ is the 2D histogram for the case that the intensity at a pixel in the portal image is a in conjunction with the event that the intensity at a pixel in the template image is b.

Enhancement of bony anatomical structures

In the current image-guided radiation therapy for prostate cancer, in general, the patient setup is performed based on the pelvic bony anatomical structures close to a target. Therefore, we investigated the effect of the enhancement of the bony structures in the pelvic DRR templates and portal images on the performance of the proposed method. Prior

to the investigation, we applied two famous edge enhancement filters, that is, the Sobel filter and Laplacian of Gaussian (LoG) [18]. As a result, the residual errors in the Euclidean distance for the Sobel filter and LoG were 2.65 $\pm$ 1.21 mm and 2.81 $\pm$ 1.2 mm, respectively, which indicated no statistically significant difference. However, it takes more time to apply the LoG filter compared with the Sobel filter. Consequently, the Sobel filter with the structure element of a 3×3 square was used for enhancement of the bony structures in this study. Kondo *et al.* [19] reported that their template matching technique with a Sobel filter was useful in preventing 'wrong' images from being stored in the correct location, for example, in the proper patient's folder in a PACS environment.

RESULTS

The actual centers in an irradiation field on the portal images were determined with high accuracy by the proposed method of searching a measuring scale using a template-matching technique. The average errors between actual centers derived from the proposed method and the gold standard actual centers were 0.3 ± 0.14 mm in Euclidean distance for the resubstitution test and 0.25 ± 0.31 mm for the validation test.

We determined the optimum size of the localized pelvic template image by investigating the effect of the template size on the residual error of the Euclidean distance in the patient setup errors. The proposed method was applied to 11 training cases. Figure 6 shows an example of localized pelvic templates for an AP and lateral views with a reduction of 100% to 40% relative size. Figure 7 shows the relationship between the relative size for the localized pelvic template image and the residual error in Euclidean distance obtained by the proposed method. The results showed that the optimum localized pelvic template size was 80% of the original localized template image that was used for estimation of the patient setup errors in this study.

Tables 1 and 2 show the residual errors for the training and test data sets, respectively, that is, the mean, SD and minimum and maximum values of residual error in the LR, SI and AP directions and for the Euclidean distance obtained by using the CC or MI, and with or without a Sobel filter. Each value was obtained by averaging the values for all cases. The proposed method using the CC with the Sobel filter achieved the minimum residual errors of 2.65 ± 1.21 mm and 3.10 ± 1.49 mm for the resubstitution and validation tests, respectively. The second minimum residual error was obtained by the method using the mutual information with the Sobel filter in both tests. Tables 3 and 4 show the P-values for statistical significance for the training and test data sets, respectively, in the residual error of the Euclidean distance between combinations of two similarity measures, that is, the CC and MI, with or without a Sobel filter. According to these results, the residual errors of the Euclidean distance by the two similarity measures with the Sobel filter were significantly smaller than those without the Sobel filter. In addition, there were no statistically significant differences in the residual errors of the Euclidean distance between the methods using the cross-correlation coefficient and mutual information with a Sobel filter ($P > 0.05$). Furthermore, there were no statistically significant differences in the residual errors in the three directions and the residual error for the Euclidean distance between the resubstitution and validation tests ($P > 0.05$).

The residual errors in the three directions (LR, SI and AP) obtained by the method using the CC with the Sobel filter were smaller than 2 mm in both tests, as shown in

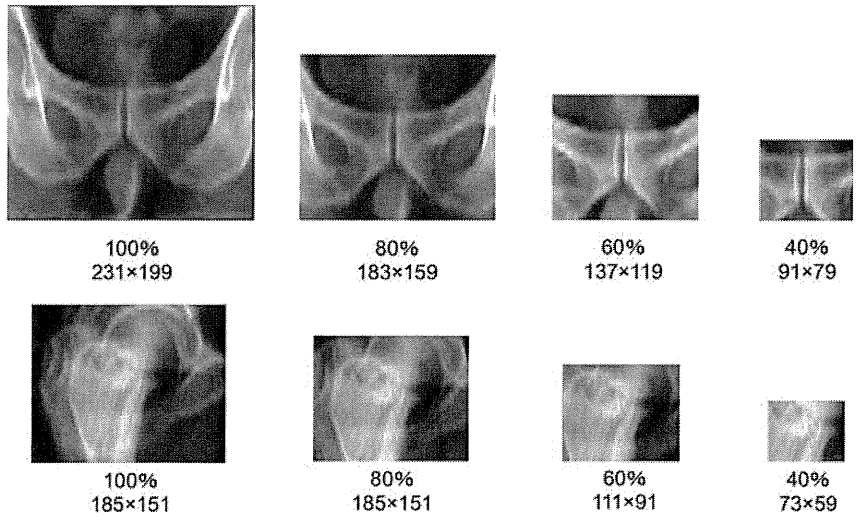

Fig. 6. An example of localized pelvic templates for an AP and lateral views with reductions of 100% to 40% relative size. The percent relative size and matrix size are shown under each template.

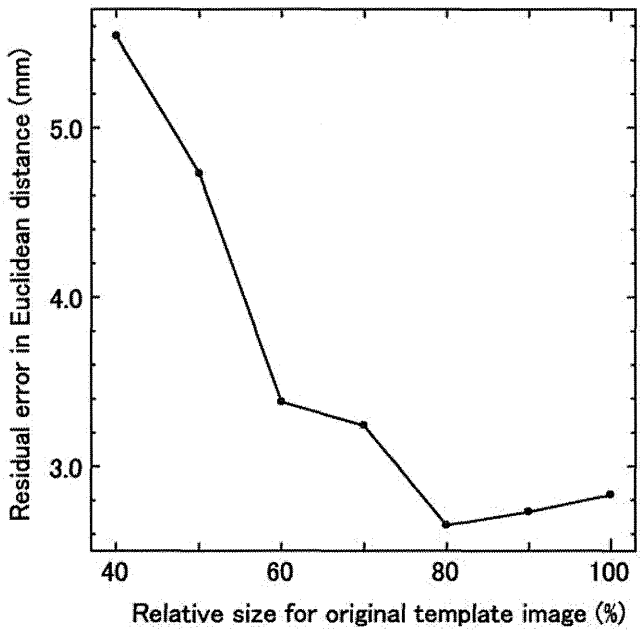

Fig. 7. Relationship between the relative size for the localized pelvic template image and the residual error in Euclidean distance obtained by the proposed method. Note that the 100% relative size for the localized pelvic template was the original pelvic template, which was automatically obtained from the patient's own DRR image by cropping a rectangular region.

Tables 1 and 2. These residual errors are smaller than a tolerance of 2 mm for imaging and treatment coordinate coincidence in the EPID, which is recommended by the American Association of Physicists in Medicine Task Group 142 [20]. Tables 5 and 6 show the *P*-values for statistical significance for the training and test data sets, respectively, in the residual error between the two directions using CC and MI with a Sobel filter. These results indicate that there were no statistically significant differences in the residual error between the two directions by either method or with either test ($P > 0.05$).

The average calculation time of patient setup errors by the proposed method was about 10 s on a personal computer with a 3.33-GHz central processing unit (Intel, Core (TM) 2 Duo) and 4.0-GB memory, excluding the production of AP and lateral DRR images, which required about 8 min on average to obtain the DRR images.

DISCUSSION

Although a number of papers have been published on the detection of patient setup errors, most of these papers have involved phantom studies rather than patient studies. We compare the proposed method with two past studies, in which the methods for detection of setup errors were applied to patient data as validation tests. Thilmann *et al.*

Table 1. The mean, SD and minimum and maximum values of residual error in the left–right, superior–inferior and anterior–posterior directions and residual error for the Euclidean distance obtained by using the cross-correlation coefficient or mutual information, with or without a Sobel filter, for a training data set

		Residual error (mm)			
Method	**Direction**	**Mean**	**SD**	**Min**	**Max**
CC	LR	1.17	0.98	0.00	4.20
	SI	1.44	1.23	0.00	4.48
	AP	6.60	3.59	1.12	11.53
	Euclidean	7.27	3.09	2.46	11.87
CC + Sobel	LR	1.33	0.93	0.56	4.20
	SI	1.28	0.98	0.00	2.80
	AP	1.58	0.86	0.00	2.81
	Euclidean	2.65	1.21	0.56	5.78
MI	LR	1.81	2.17	0.00	6.99
	SI	4.56	3.43	0.56	9.53
	AP	4.68	3.69	0.56	9.85
	Euclidean	8.25	2.84	3.23	13.43
MI + Sobel	LR	1.33	0.93	0.56	4.20
	SI	1.28	0.98	0.00	2.80
	AP	2.14	2.23	0.00	9.57
	Euclidean	3.13	2.23	0.56	9.84

LR = left–right; SI = superior–inferior; anterior–posterior = AP; CC = cross-correlation coefficient; MI = mutual information.

[6] developed a reliable workflow from image acquisition to correction of interfraction setup errors using kV cone beam CT (CBCT). In their method, the registration between the CBCT with the planning CT is achieved by using an automatic matching algorithm that maximizes mutual information. In their application of the automatic registration to two prostate cancer patients, the mean residual error was 3.2 mm. Wierzbicki *et al.* [10] proposed two fully automatic image-guided radiotherapy (IGRT) techniques, that is, 'forward' and 'reverse' IGRT techniques, based on a linac-integrated CBCT system that requires a significantly smaller imaging dose. When using the reverse technique, which involves non-rigid deformation of the planning CT and contours to match the CBCT, their image guidance method showed a mean residual error of 3.3 mm for prostate cancer in 10 patients while requiring only 20% of the standard imaging dose. On the other hand, our results showed that the mean residual error was 3.1 mm for the validation test with 10 cases, which seems to be comparable with past studies.